Case Studies in Thermal Engineering 60 (2024) 104691

Contents lists available at ScienceDirect

Case Studies in Thermal Engineering

journal homepage: www.elsevier.com/locate/csite

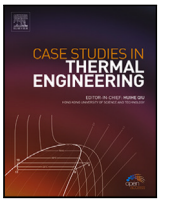

Performance comparison of sCO_2 and steam cycles for waste heat recovery based on annual semi-transient modeling under complex industrial constraints

Vincent Thielens [a,b,*], Frederiek Demeyer [b], Ward De Paepe [a]

[a] Thermal Engineering and Combustion Unit, University of Mons, rue de l'Épargne 56, Mons, 7000, Belgium
[b] Mechanics and Thermal processes, Engie R&I Laborelec, Rodestraat 125, Linkebeek, 1630, Belgium

HIGHLIGHTS

- design of a sCO_2 cycle for heat and power production from a municipal waste incinerator.
- review on the models of sCO_2 components with off-design behavior.
- thermodynamic comparisons between sCO_2 and steam cycle.
- economical assessment of the capital expenditure and levelized cost of electricity.
- sCO_2 cycle is more advantageous for this waste heat recovery application than the conventional steam setup.

ARTICLE INFO

Keywords:
sCO_2 cycles
Waste heat recovery
Semi-transient
Cogenerative application
Exergy efficiency
Economic assessment
Levelized cost of electricity

ABSTRACT

The increasing demand for energy efficiency is compelling industries to seek ways to save energy. Waste heat recovery plays a crucial role by optimizing fuel usage through combined heat and power generation. In recent decades, sCO_2 technologies have emerged as potential contenders to traditional steam cycles. However, there is a noticeable gap in literature regarding case studies on integrating off-design behaviors of components in complex industrial environments. To address this gap, this study focuses on a specific scenario involving a waste incinerator already linked to a steam generator within a cogeneration setup, alongside a flue gas cleaning unit. The conventional steam bottoming cycle is innovatively replaced with an sCO_2 cycle, and a comparison between the performance of the existing steam technology and a numerical sCO_2 model is conducted. This comparison involves modeling the off-design behaviors of each component run hourly over a one-year period. Results show that the sCO_2 setup increases the electric power generation by 25% with the global efficiency around 43%, compared to the initial 37.3%. These outcomes answer a need in literature by showing that, even in off-design, the higher exergy efficiency of the sCO_2 setup is more advantageous. Unlike steam evaporation at constant temperature, sCO_2 is less constrained by temperature limitations in the heater and allows for higher turbine inlet temperatures. Additionally, an economic assessment reveals a levelized cost of electricity between 8.5 and 16.7 $/MWh_e$. However, further advancements in component modeling and enhanced energy recovery from cooler/exhaust gases are identified as areas for future research.

* Corresponding author at: Thermal Engineering and Combustion Unit, University of Mons, rue de l'Épargne 56, Mons, 7000, Belgium.
E-mail address: vincent.thielens@umons.ac.be (V. Thielens).

https://doi.org/10.1016/j.csite.2024.104691
Received 23 February 2024; Received in revised form 27 May 2024; Accepted 11 June 2024
Available online 13 June 2024

Nomenclature		
Acronyms	CAPEX	Capital expenditure
	CEPCI	Chemical engineering plant cost index
	IGV	Inlet guide vane
	LCOE	Levelized cost of electricity
	PCHE	Printed circuit heat exchanger
	PFHE	Plate fin heat exchanger
	sCO_2	Supercritical carbon dioxide
	WHR	Waste heat recovery
Greek letters	η	Energy efficiency [%]
	λ	Thermal conductivity [W/m K]
	μ	Dynamic viscosity [Pa s]
	Π	Pressure ratio [ ]
	ψ	Exergy efficiency [%]
	ρ	Density [kg/m^3]
	ζ	Colebrook's friction factor [ ]
Roman letters	c_p	Specific heat capacity [J/kg K]
	h	Enthalpy [J/kg K]
	U	Thermal transmittance [W/m K]
	Nu	Nusselt number [ ]
	Pr	Prandtl number [ ]
	Re	Reynolds number [ ]
Subscripts	$_b$	Property evaluated at the bulk temperature
	cold	Property evaluated at the cold side
	e	Electrical
	hot	Property evaluated at the hot side
	lam	Laminar
	th	Thermal
	turb	Turbulent
	$_w$	Property evaluated at the wall temperature

1. Introduction

The accomplishment of efficient systems facilitating sustainable and optimal energy utilization has emerged as a primary objective for an increasing number of companies. In many fields of engineering, innovations are brought to either decrease the consumption of fossil energy, or better valorize renewable sources. However, Johnson [1] estimates that between 20% and 50% of the primary energy input in U.S. industrial processes is lost as waste heat, with up to 40% potentially recoverable as useful work. Waste heat recovery (WHR) technology thus presents a compelling opportunity to reduce industrial carbon footprints. The WHR also complies with the United Nations' sustainable development objectives by contributing to the rational use of energy.

While there is a growing interest in publications focusing on sCO_2 cycles [2], the integration of off-design behavior into long-term numerical performance analyses remains a gap, as highlighted by the key findings in Table 1. While the potential of sCO_2 cycles for WHR has been explored [3–5], few studies have delved into off-design performance [6]. Furthermore, the combined heat and power application using supercritical cycles mainly focuses on gas turbine exhausts [7] and the assessment of the potential of municipal waste incinerators with sCO_2 cycles are not frequent [8]. Additionally, the lack of industrial-scale components for sCO_2 applications complicates cost estimations, hindering the implementation of pilot plants for waste heat recovery, as advocated by initiatives like the CO_2OLHEAT consortium [9].

Addressing this gap, this study focuses on a case study involving a waste incinerator. In this setting, waste heat from combustion is currently recovered via a steam cycle, producing electricity and cogenerated steam. This study numerically replaces the steam cycle with an sCO_2 cycle while maintaining cogeneration to show the potential of sCO_2. However, the singular nature of flue gases necessitates a cleaning unit, imposing constraints on heater outlet temperature and complicating cycle optimization. With this study, we aim to assess the potential of sCO_2 power cycles in industrial environments with thermal constraints as well as combined heat and power need.

In this study, the best sCO_2 cycle is first identified and it is presented how it suits to the hot temperature curve, followed by a review of component modeling and an assessment of overall plant performance. Initial simulations under nominal conditions characterize component features such as heat transfer coefficient, area, and enthalpy rise. Subsequently, off-design component characteristics are defined, and simulations are conducted over a one-year time frame. An economic assessment of the plant is then performed, discussing estimations of the levelized cost of electricity. The different aspects that have been left for future work are finally presented. By presenting the techno-economical results of a sCO_2 setup simulated during one-year with the off-design

Table 1
Among the different key findings presented in literature, none of them propose a setup for combined heat and power in a waste incinerator while taking into account the off-design characteristics.

References	Main outcomes
[2]	sCO_2 cycles are cost effective
	sCO_2 are suitable for high-temperature sources (>350 °C)
	sCO_2 efficiencies for industrial WHR can reach 27.9%
[3]	Net efficiency for preheating cycle can reach 28.3%
	Design of sCO_2 cycles for GT exhaust
[4]	Lack of pilot plants for more than 10 MW_e
[5]	Design of sCO_2 cycles with efficiencies up to 27.7%
[6]	Investigation of the off-design performance of a sCO_2 cycles
[7]	Identification of different location to recover heat on a sCO_2 setup
[8]	Integration of a sCO_2 cycle on a coal-fired power plant with waste incineration
[9]	Design of a sCO_2 cycle for waste heat recovery
[10]	Design of a sCO_2 cycle on a coal-fired power plant

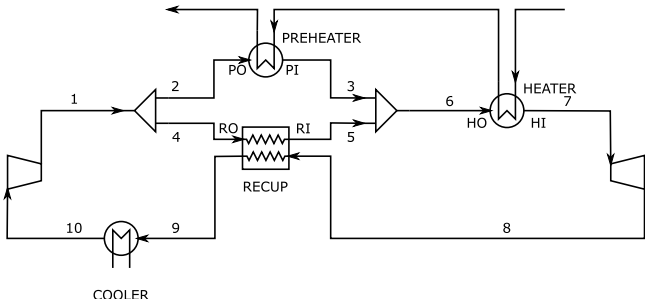

Fig. 1. The preheating cycle is an highly recuperative cycle achieving high net power production with a limited number of components.

characteristics of the components, this paper answers the lack of case studies in literature and promotes the development of sCO_2 cycles.

2. Methodology

Within the array of sCO_2 cycle configurations, a specific design is chosen for its ability to be close to the hot source temperature curve compared to traditional steam cycles, thereby enhancing both the quality and quantity of recovered heat. Additionally, supercritical carbon dioxide exhibits behaviors noticeably distinct from conventional industrial fluids like water and air, offering potential advantages for power cycle applications. However, the considerable property variations near the critical point pose challenges in component simulation. The accuracy of computations thus relies on the synergy between equation of state and components modeling. This section begins by presenting the cycle configuration and the technological selections for components simulation, followed by the equation of state adopted for sCO_2 modeling. Finally, various performance indicators are delineated to facilitate cycle performance assessment.

2.1. Design of the sCO_2 cycle

In the realm of waste heat recovery, the primary objective is to maximize electric power production based on the energy source derived from industrial processes. However, the heat characteristics released by these processes fluctuate according to plant activity, necessitating an additional power cycle with good flexibility to accommodate these variations. Moreover, industries seek low-cost power cycles that do not disrupt the stability of their primary operations. This means the proposed cycle should independently adapt to process variations and be low in capital expenditure (CAPEX), both of which are fulfilled by sCO_2 cycles.

Among the various cycles outlined in Crespi's comprehensive review [11], the preheating cycle emerges as one of the most promising for WHR applications. In this cycle, illustrated in Fig. 1, the flow is split into two streams after compression. These substreams are then separately heated, one in the preheater and the other in the internal recuperator. Subsequently, the heated flows are mixed and further heated in the heater. The energy content is recovered through expansion in the turbine, with any remaining potential energy recuperated in the recuperator before being released to the environment via a cooler.

The preheater optimally adjusts the isobaric curve of exhaust gases to the heating curve of sCO_2, adding a degree of freedom to cycle optimization. By exploiting the variation of CO_2 specific heat capacity (c_p) with temperature through split flows, the cycle enhances recuperation potential. Economically, the preheating cycle offers simplicity compared to cascade cycle configurations, leading to favorable Levelized Cost of Electricity (LCOE) and enabling industrial owners to constrain investments.

Table 2
The mean molar composition of the exhaust gases fluctuates between minimal and maximal concentration levels.

Components		min	mean	max	
Nitrogen	N_2	57.7	67.9	74.9	%
Water	H_2O	12.5	16.1	20.8	%
Carbon dioxide	CO_2	7.9	9.1	10.3	%
Oxygen	O_2	4.7	6.9	11.2	%

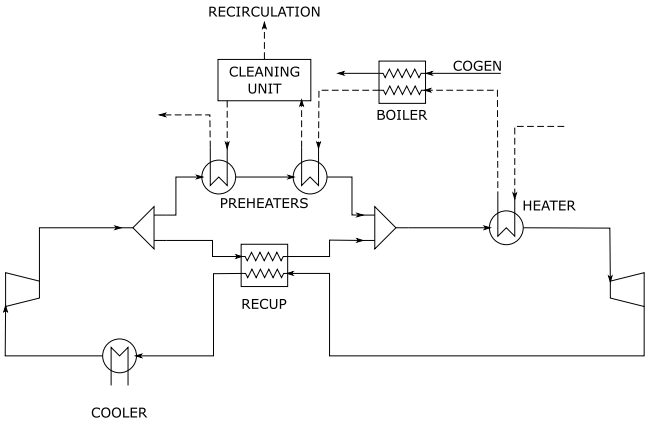

Fig. 2. In this adapted configuration, an additional preheater has been added to recover heat before and after the cleaning unit.

Waste heat recovery regroups a wide variety of categories needing to be considered separately. In the frame of the municipal waste incinerator considered, three elements are constraining the design of a novel sCO_2 setup. The fluctuations in terms of composition and flow rate of the exhaust gases firstly forces the setup to be flexible to follow the recoverable potential. Furthermore, the exhaust gases from an incineration furnace are corrosive and contain many pollutants requiring important cleaning (such as $deNO_x$, $deSO_x$ and filters). In addition to the combined heat and power requirement, those aspects constraint the optimization of the cycle. This paper delves into a genuine industrial scenario, encompassing all pertinent process constraints that add complexity to cycle optimization, such as the cogeneration arrangement with a neighboring company and the thermochemical constraints imposed by a cleaning unit. Due to confidentiality concerns, detailed descriptions of the cogeneration characteristics cannot be provided.

The initial evaporator operates to recover heat from exhaust gases with temperatures ranging between 550 °C and 750 °C, under nearly atmospheric pressure, with a composition detailed in Table 2. To comply with environmental regulations, the system incorporates a flue gas treatment unit. Depending on the installation's chemical requirements (namely, $deNO_x$ and $deSO_x$), the exhaust gases must enter the cleaning unit at 210 °C and exit at 190 °C. Additionally, a portion of the exhaust gases is recirculated within the process, resulting in only half of the original 300–600 t/h of flue gases being present after passing through the cleaning unit for further heat recovery.

The preheating cycle depicted in Fig. 1 requires adaptation through the incorporation of an additional preheater following the boiler for cogeneration, as illustrated in Fig. 2. The temperature of the exhaust gases post-boiler is sufficiently high to permit further heat recovery before reaching the cleaning unit. As depicted in Fig. 3, the selected configuration aims to closely align the cold curve with the hot curve, considering the constraints posed by pinches. Consequently, the Ts diagram in Fig. 4 for the sCO_2 curve closely mirrors that of the flue gases, maximizing exergy recovery. Although reducing the sCO_2 mass flow rate elevates its temperature at the heater outlet, this adjustment would not necessarily enhance performance. It is crucial to strike a balance between turbine inlet temperature and mass flow to optimize overall performance.

2.2. Model of the components

The preheating cycle depicted in Fig. 1 reduces the number of components compared to its steam counterpart, omitting essentials like the deaerator and hot pot. Moreover, the turbomachinery is downscaled owing to the higher density of CO_2 in its supercritical phase. Nonetheless, the considerable fluctuations in the physical characteristics of sCO_2 around its supercritical point necessitate careful consideration in component design. Consequently a concise examination of the requisite components and their modeling becomes imperative. Primarily, attention is directed towards the compressor, turbine, and heat exchanger in this overview.

2.2.1. Compressor

The compressor begins its operation by taking gas at 33 °C and 85 bar to raise it to a pressure of 280 bar. With compression power below 10 MW, the radial architecture emerges as the most suitable choice, as highlighted in a review by White [2]. Assuming

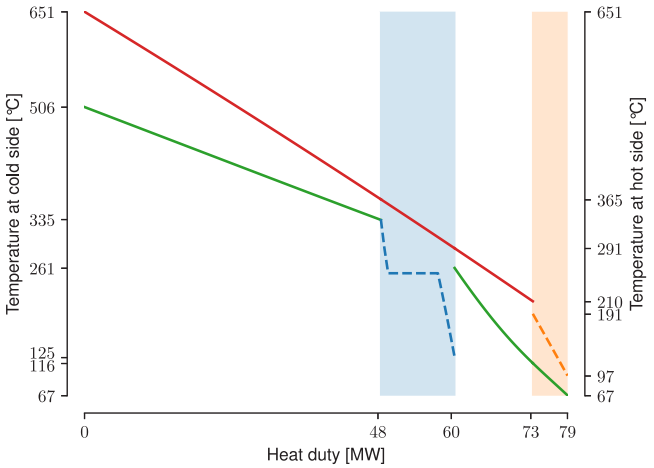

Fig. 3. The high recuperativeness of the preheating cycle allows the hot curve temperature to be closed to the cold one. The exhaust gases curve before and after the cleaning unit have respectively be drawn in plain red and dashed orange, whereas the steam is in dashed blue. (For interpretation of the references to color in this figure legend, the reader is referred to the web version of this article.)

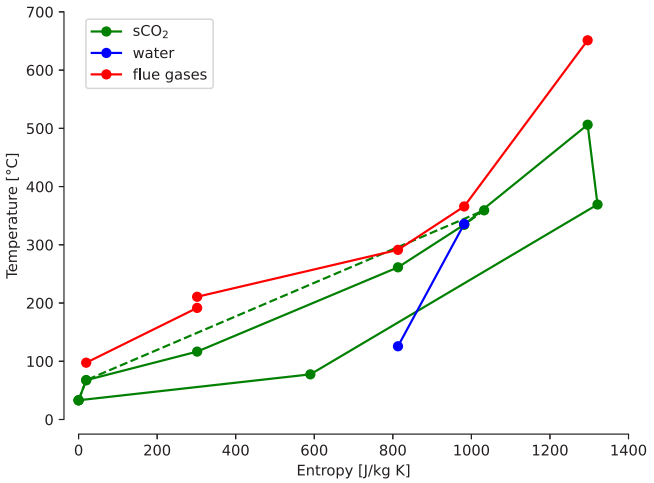

Fig. 4. On the Ts diagram of the cyle, both sCO_2 (in green), the flue gases (in red) and the steam (in blue) are depicted. The dashed green line refers to the flow through the recuperator. The curves representing flue gas and water have been adjusted on the entropy axis to facilitate a meaningful comparison with sCO_2. (For interpretation of the references to color in this figure legend, the reader is referred to the web version of this article.)

Table 3
A literature review on the compressors for sCO_2 shows that an isentropic efficiency of 80% can be expected [3,12–14].

P_{comp} MW	T_{in} °C	p_{in} bar	p_{out} bar	$\dot{m}$ kg/s	η_{is} %	Reference
1.1	32	85	216.9	45.52	73	[12]
2.7–3.5	32	77	240	110–120	82	[3]
12–17	32	75	250	315–430	88	[13]
12–27	32	70–120	300	310–640	85	[14]

an isentropic efficiency of 80% aligns with literature findings (Table 3). In a technical report authored by Alfani [12], Baker Hughes presents performance maps for two compressors arranged in series. These compressors intake gas at 32 °C and 85 bar, achieving a pressure ratio of 2.55. The maps detail the variations in efficiency η/η_{nom} and enthalpy rise $\Delta h/\Delta h_{nom}$ across different inlet guide vane angles, ranging from −60° to 10°. Fig. 5 correspond to the first and second compressors utilized in Alfani's study [12].

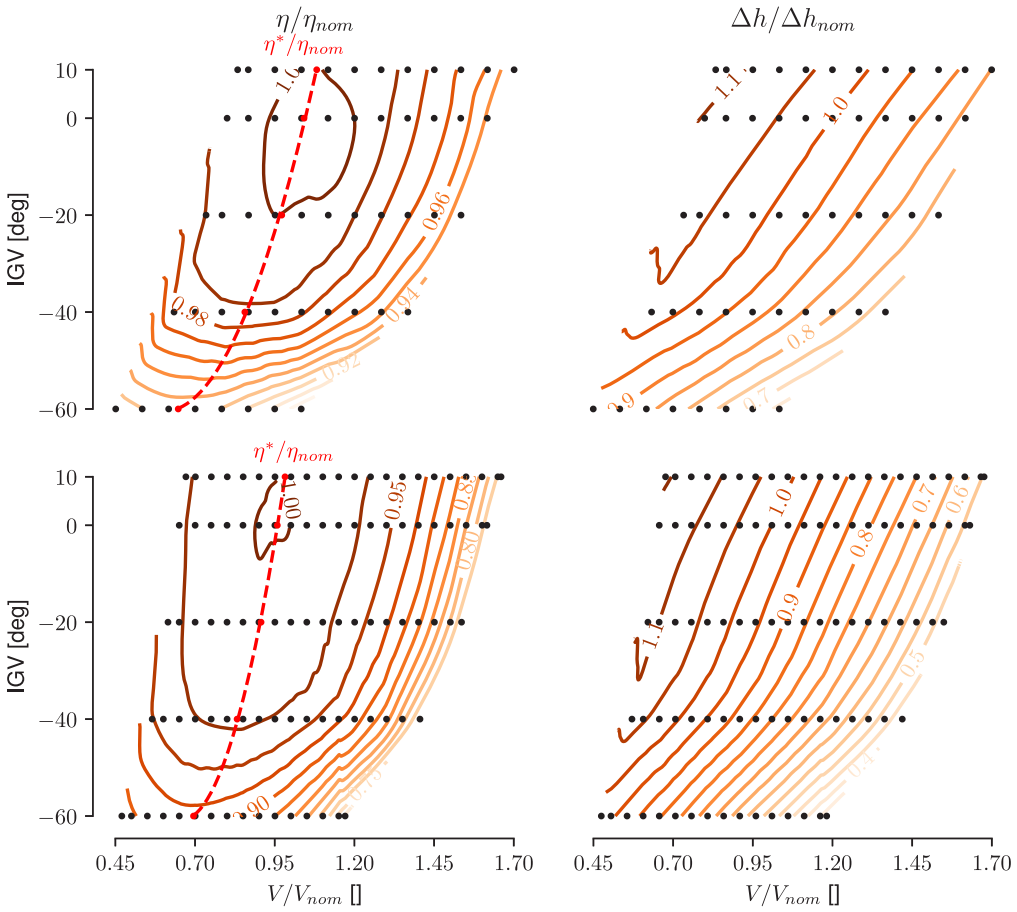

Fig. 5. Alfani [12] presents the normalized operating maps of the first (above) and second (below) compressors. Only the black dots are given as data in its study for inlet guide vanes between −60° and 10°, the maps are obtained by interpolation.

Table 4
A literature review on the turbines for sCO_2 shows that an isentropic efficiency of 90% can be expected [3,13,14].

P_{turb} MW	T_{in} °C	p_{in} bar	p_{out} bar	$\dot{m}$ kg/s	η_{is} %	Reference
6.7–10	410–483	238	79	93–120	85	[3]
46–63	500	250	75	315–430	92	[13]
53–96	370–530	300	70–80	310–640	90	[14]

2.2.2. Turbine

The turbine expands the flow of sCO_2, converting thermal energy into mechanical energy. In the realm of sCO_2 turbines, two classifications exist: axial and centrifugal. Considering the power fluctuations of the chosen application, ranging between 20 MW and 40 MW, the axial configuration emerges as the most suitable choice [2]. Examining literature values (Table 4), a 90% isentropic efficiency can be reasonably assumed. Siemens offers performance curves for its power turbine detailed by Alfani [12]. These dimensionless curves depict the normalized reduced mass flow rate (Eq. (1)) and the normalized isentropic efficiency relative to the normalized pressure ratio. Due to the anticipated operation of the turbine at the same rotational speed as the electrical grid frequency, only a single curve is utilized. Quadratic interpolation techniques are applied to effectively fit the data for integration within the semi-transient model.

$$\dot{m}_{red,\ turb} = \dot{m}\frac{\sqrt{T_{in,\ turb}}}{p_{in,\ turb}} \tag{1}$$

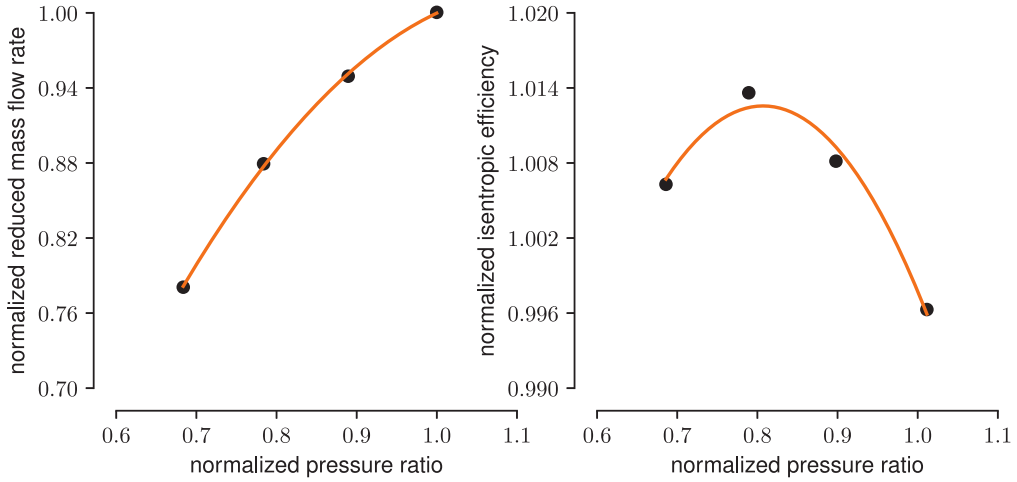

Fig. 6. In its work, Alfani [12] presents the normalized operating maps of the turbine used in this case study.

2.2.3. Heat exchange with the exhaust gases

The process of heat exchange between supercritical carbon dioxide (sCO_2) and industrial waste gases occurs within the heaters and preheaters. These heat exchangers can be categorized based on the predominant heat transfer mechanisms, either a combination of radiation and convection or convection alone. In waste heat recovery applications, convection-based exchanges are prevalent, with commonly mentioned configurations including shell and tube designs, micro-tubes, and plate-fin structures [2]. However, the presence of particulate matter in the exhaust gases can quickly lead to fouling issues, necessitating the consideration of cleaning technologies such as mechanical and ultrasound methods.

Additionally, the high temperatures (up to 800 °C) and the presence of solid particles significantly increase the contribution of radiative heat transfer phenomena. Consequently, configurations where sCO_2 flows within tubes or microtubes while gases flow outside are favored.

To model heat transfer within the tubes, the correlation developed by Krasnoshchekov and Protopopov is particularly notable for its effectiveness with supercritical carbon dioxide [4,15]. Furthermore, Jackson's work [16] demonstrates that employing the Dittus-Boelter's correlation with appropriate modifications yields satisfactory results when compared against empirical data. The Dittus-Boelter's correlation (Eq. (2)) expresses a proportionality relation for the Nusselt number: $Nu \propto Re^{0.8}$.

$$Nu_b = 0.023 Re_b^{0.8} Pr_b^{0.5} \left(\frac{\rho_w}{\rho_b}\right)^{0.3} \quad [16] \tag{2}$$

The equation governing the pressure drop in pipes with circular cross-section is provided by Eq. (3), wherein ζ' represents the corrected friction factor, denoted as ζ, according to Colebrook's formula (as shown in Eq. (4) and Eq. (5)) [4,17,18].

$$\Delta p = \zeta' \frac{l}{d_i} \frac{\rho v_i^2}{2} \tag{3}$$

$$\frac{1}{\sqrt{\zeta}} = -2 \log\left(\frac{2.51}{Re\sqrt{\zeta}} + \frac{K}{3.71 d_i}\right) \quad [17] \tag{4}$$

$$\frac{\zeta'}{\zeta} = \left(\frac{T_b}{T_w}\right)^{0.1} \quad [17] \tag{5}$$

Gnielinski's correlations [19] provide an average Nusselt number for cross-flow over tubes on the outside of the tubes. This average Nusselt number (Eq. (8)) is a combination of laminar (Eq. (6)) and turbulent contributions (Eq. (7)). However, for the sake of simplicity, turbulent flow is assumed, resulting in the proportional relation $Nu \propto Re^{0.8}$ for the Nusselt number. In the simulations, pressure losses on the shell side are not directly computed but are accounted for using the initial values returned by the sensors in the steam heat exchanger configuration.

$$Nu_{\text{lam}} = 0.664 Re^{0.5} Pr^{1/3} \quad [19] \tag{6}$$

$$Nu_{\text{turb}} = \frac{0.037 Re^{0.8} Pr}{1 + 2.443 Re^{-0.1} \left(Pr^{2/3} - 1\right)} \quad [19] \tag{7}$$

$$Nu = 0.3 + \sqrt{Nu_{\text{lam}}^2 + Nu_{\text{turb}}^2} \quad [19] \tag{8}$$

Table 5
The correlations provided by Meshram [22] for a straight channel allows to compute the Nusselt number and the friction factor.

Side	T_b range	Nusselt number Nu	Friction factor f
Hot fluid	500 °K < T_b < 630 °K	$0.0493 Re^{0.77} Pr^{0.55}$	$0.8386 Re^{-0.5985} + 0.00295$
Hot fluid	600 °K < T_b < 730 °K	$0.0514 Re^{0.76} Pr^{0.55}$	$0.8385 Re^{-0.5978} + 0.00331$
Cold fluid	400 °K < T_b < 500 °K	$0.0718 Re^{0.71} Pr^{0.55}$	$0.8657 Re^{-0.5755} + 0.00405$
Cold fluid	500 °K < T_b < 600 °K	$0.0661 Re^{0.743} Pr^{0.55}$	$0.8796 Re^{-0.5705} + 0.003533$

2.2.4. Exchange between sCO_2 and sCO_2

Incorporating an internal heat exchanger significantly enhances the efficiency of the cycle by reclaiming a substantial portion of energy before the fluid undergoes cooling in the cooler, a point elaborated upon later. For instance, the heat exchanged within the recuperator can surpass the heat recovered from the source. Among the various compact heat exchanger technologies outlined in Kwon's research [18], printed circuit heat exchangers (PCHEs) stand out as the most prevalent choice for sCO_2 recuperators [2]. In PCHEs, individual channels are fabricated through chemical etching onto metal plates and subsequently stacked together. The high stacking pressure facilitates diffusion bonding of the channels, forming a solid block capable of withstanding a wide pressure and temperature range (up to 500 bar and 800 °C, respectively). However, the inability to disassemble PCHEs poses challenges for cleaning and maintenance procedures. Consequently, PCHEs are best suited for non-fouling environments and prove ideal for sCO_2/sCO_2 recuperators where the flows remain clean.

Various channel designs with differing levels of complexity (such as straight, zigzag, s-shaped, airfoil) have been developed [20,21], resulting in diverse correlations for the Nusselt number and friction factor, as summarized by Kwon and White [2,18]. In this investigation, Meshram's correlations [22] for straight channels are employed, as detailed in Table 5.

2.2.5. Exchange between sCO_2 and air

The function of the cooler is to reduce the temperature of the sCO_2 flow at low pressure to near its critical temperature, thereby minimizing the power needed for compression. This cooling can be achieved either through air or water. In waste heat recovery applications, where a water supply may not always be accessible, air cooling is a more versatile assumption. The plate fin technology stands out as the most suitable option due to its higher heat transfer coefficient on the sCO_2 side [18]. This technology consists of fins and plates brazed together to create a surface density of up to 5000 m^2/m^3 [23]. However, fouling sensitivity is a notable concern with this design.

In the design model, it is assumed that the available cold source can consistently cool sCO_2 to 33 °C by adjusting the air flow rate, a temperature well within the achievable range of 32–36 °C presented in Moisseytsev's work [24]. During periods of high ambient temperatures, the mass flow through the compressor may be restricted, leading to a reduction in power output. This limitation is observed even in steam Rankine cycles and is thus acceptable for sCO_2 substitutes.

In the subsequent simulations, the power required by the cooler fans in the steam case is assumed to be comparable to that in the sCO_2 cycle. While it constitutes 10% of the power output in the steam reference case, Moisseytsev [24] suggests it could potentially be reduced to 5% of the power output. Adopting the hypothesis of equal fan power requirements in both cases (steam and sCO_2) is therefore a more conservative approach. Thus, adhering to Moisseytsev's hypothesis presents an additional advantage of sCO_2 cycles over steam. Nonetheless, a more detailed design of the cooler is reserved for future endeavors.

2.3. Equation of state

The behavior of carbon dioxide exhibits significant variations around its critical point, which is at 30.978 °C and 73.773 bar [4]. Employing an accurate equation of state becomes crucial to avoid erroneous calculations, especially for components operating near this critical region, such as the compressor inlet or the low-pressure side of the recuperator. Among the most precise equations of state for pure CO_2 is the Span-Wagner's model [25,26], which offers a broad coverage across temperatures ranging from −57 °C to 826 °C and pressures ranging from nearly 0 bar to 8000 bar.

In power cycle applications, typical operating conditions fall within the range of 85/300 bar for pressure and 30/600 °C for temperature. Within this range, the Span-Wagner's model predicts uncertainties in density and isobaric heat capacities not exceeding 0.1% and 2%, respectively. Although extrapolating beyond this range introduces increasing uncertainties, the Span-Wagner's model remains adequate for power cycle applications.

Refprop, which incorporates the Span-Wagner's equation of state, is utilized for all simulations in this study, while Aspen Plus serves for thermodynamic computations [27].

2.4. Performance evaluation metrics

To compare the sCO_2 configuration against the initial steam cycle, it is necessary to establish certain performance metrics. However, evaluating performance in the context of waste heat recovery is not as straightforward as in traditional power plants due to their inherent particularities. The waste incineration sector mandates the cleaning of exhaust gases before release into the atmosphere, necessitating the integration of these constraints while maintaining objectivity in performance assessments. Furthermore, the presence of a combined heat and power setup implies to take into account both electrical and thermal production. Additionally, proper characterization of efficiency requires comparing the electrical power generated to the thermal exergy. After decoding the distinctions between sensible heat and heat flux, the computations of these indicators are presented below.

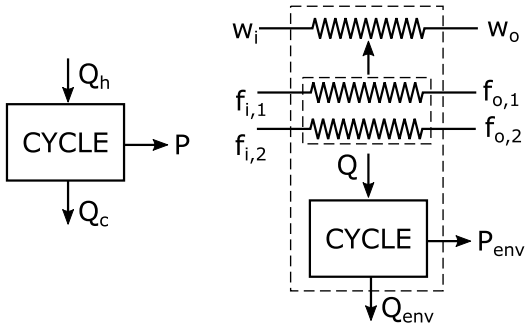

Fig. 7. The schematic representation of a power cycle converts an amount of heat Q_h to power P by releasing a given amount of heat to the cold source Q_c. The analyzed case can be represented with the dashed box where both power and heat (trough steam production w) are valorized, taking into account the exhaust gases flowing in (f_1) and out (f_2) of the cleaning unit.

2.4.1. Distinction between sensible heat and heat flux sources

A thermodynamic power cycle can be represented schematically by a box (refer to Fig. 7), wherein heat from a hot source Q_h is transformed into power P by releasing a quantity of heat Q_c to a cold source. The efficiency (Eq. (9)) is conventionally calculated as the ratio of the power generated to the heat flux extracted from the hot source.

$$\eta = \frac{P}{Q_h} = \frac{P}{Q_h} = 1 - \frac{Q_c}{Q_h} \tag{9}$$

Efficiency serves as a common metric for categorizing cycles, with the ideal cycle being the one achieving the highest efficiency. This approach is valid when dealing with a heat flux source because the cost is directly tied to the hot heat flux (e.g., flux derived from a nuclear reaction). The primary objective of a power cycle is thus to maximize the power produced P for a given flux Q_h, which is equivalent to maximizing the efficiency η. Utilizing efficiency enables comparison between different cycle technologies through a dimensionless representation of power output.

However, this line of reasoning may not be suitable for sensible heat sources encountered in waste heat recovery scenarios. Unlike a heat flux source, a thermochemical process offers an energetic source that may not be fully utilized. To illustrate, in a waste incinerator, the primary objective is to incinerate non-recyclables, with the recovery of a portion of the released heat considered a secondary concern. In this context, the thermal flux recovered Q_h is not fixed, and maximizing power (Eq. (10)) involves optimizing two parameters: the cycle efficiency η and the heat flux recovered Q_h at the source.

$$P = \eta Q_h \tag{10}$$

In any case, whether dealing with a heat flux source or a sensible heat source, the objective remains consistent: to generate maximum power under given conditions. In the case of a heat flux source, achieving maximum power is equivalent to optimizing efficiency because Q_h remains constant. However, this assessment no longer holds true for a sensible heat source, where both the efficiency η and Q_h must be optimized to attain optimal performance. The concept of efficiency, rooted in an energetic perspective, may not be the most pertinent in waste heat recovery scenarios. Consequently, to compare different cycle technologies, the power produced should not be normalized based solely on the enthalpy flux entering the cycle, but rather with the exergy flux of the flue gases. The concept of exergy, as elucidated by Dincer [28], holds particular significance in such computations.

2.4.2. Performance metric

As outlined in Dincer's study [29], the utilization of exergy efficiency ψ offers numerous benefits by indicating the proximity of the cycle to the theoretical limit set by Carnot's law. Exergy losses determinate where the primary work potential is squandered, with a high energy loss not necessarily correlating with a substantial amount of recoverable work.

In the context of a cogeneration power plant (Fig. 7), the valorization of heat must be factored into efficiency computations. For energy efficiency η, the valuable outputs comprise both the cogenerated heat and power (the numerator of Eq. (11)), while the input cost constitutes the heat flux required by the system (the denominator of Eq. (11)). To maintain objectivity, the penalty incurred by the cleaning procedure should be excluded, as the legal obligation to clean gases results in an energy loss unrelated to the cycle's performance.

$$\eta = \frac{P_{env} + \dot{m}_w(h_{w,o} - h_{w,i})}{\dot{m}_{f,1}(h_{f,i,1} - h_{f,o,1}) + \dot{m}_{f,2}(h_{f,i,2} - h_{f,o,2})} \tag{11}$$

From an exergetic perspective, the exergy efficiency ψ is calculated with a subtle variation (Eq. (12)). In contrast to efficiency η, the cost is represented by the exergy consumed by the system, while the outputs consist of both the power generated and the exergy transferred to the water flow.

$$\psi = \frac{P_{env} + \dot{m}_w(j_{w,o} - j_{w,i})}{\dot{m}_{f,1}(j_{f,i,1} - j_{f,o,1}) + \dot{m}_{f,2}(j_{f,i,2} - j_{f,o,2})} \tag{12}$$

Table 6
Design specifications chosen for the components under nominal characterization.

Compressor	T_{in}	33	°C
	p_{in}	85	bar
	p_{out}	280	bar
	η_{is}	80	%
Turbine	p_{in}	280	bar
	p_{out}	85	bar
	η_{is}	90	%
Steam generator	Δp	0	bar
	Temperature pinch	30	°C
Heater	Δp	0	bar
	Temperature pinch	30	°C
Preheater 1	Δp	0	bar
	Temperature pinch	30	°C
Preheater 2	Δp	0	bar
	Temperature pinch	30	°C
	Outlet hot temperature	$T_{cleaning}$	°C
Recuperator	Δp	0	bar
	Temperature pinch	10	°C
Cooler	Δp	0	bar
	Outlet temperature	33	°C

Once the flow is discharged into the environment via the stack at an imposed temperature, further heat recovery and conversion into energy come to an end. To address this, we can adjust the exergy computation (Eq. (13)) by excluding the output exergy term $j_{f,o,2}$.

$$\psi_{25} = \frac{P_{env} + \dot{m}_{w}(j_{w,o} - j_{w,i})}{\dot{m}_{f,1}(j_{f,i,1} - j_{f,o,1}) + \dot{m}_{f,2} j_{f,i,2}} \tag{13}$$

The definitions of these three indicators (η, ψ, and ψ_{25}) allow for a clear characterization of the simulation results while maintaining objectivity regarding the imposed penalties.

3. Results and discussion

Based on the performance characteristics outlined for the components, the cycle undergoes simulation over the course of one year on an hourly basis, utilizing data supplied by the waste incinerator. Initially, the components are depicted under their nominal operating conditions to gain insight into their achievable performances. After evaluating these performances, the components can be depicted more accurately (e.g., area, heat transfer coefficient) for off-design simulations.

3.1. Performances under nominal characteristics

In the nominal simulation, the components are evaluated to operate under ideal conditions (i.e., best efficiency without pressure drop), as detailed in Table 6. These assumptions are drawn from literature as representative of achievable technological performances. Regarding the turbomachinery, the selected efficiencies align with the state-of-the-art findings presented in the previous section. Furthermore, operating within the range of 85 to 280 bar is considered technologically feasible [4]. Within this section, it is assumed that the flow rate does not influence the performances of the components. Consequently, this approach aids in identifying the ranges of inputs (e.g., temperature, flow rate, pressure, heat flux) that the components must accommodate. To establish an upper bound for these required characteristics, particularly for turbomachinery, the pressure losses in the components are not taken into account.

The hourly operational data of the plant serve as input for simulating the environment of the sCO_2 setup. To ensure fidelity to real-world conditions, the simulated sCO_2 cycle mirrors the temperature, flow rate, and pressure of the waste heat source from the initial steam cycle. Additionally, cogeneration demand and condensate return are incorporated as input variables for the sCO_2 cycle, while a constraint is imposed on the temperature at the inlet of the cleaning unit.

Upon simulating the performance of the sCO_2 cycle over a one-year period and comparing it with the reference case, results reveal that the preheating cycle yields an average surplus of 5.8 MW_e compared to the initial steam cycle (Fig. 9). This discrepancy in power production can be attributed to the superior potential of the supercritical cycle in waste heat recovery. Fig. 8 elucidates the sources of discrepancy among the components. Specifically, the sCO_2 cycle recovers an additional 6 MW_{th} from the hot source, while emitting 5 MW_{th} less to the environment. Furthermore, the sCO_2 turbine generates 15 MW_e more than the steam turbine, with only 7 MW_e required for CO_2 recompression.

Notably, the balance on the steam reference at Fig. 8 (pumping power and hot flux as inlet, turbine power and cold flux as outlet) does not equilibrate, with a relative difference of 4.9%. This discrepancy arises from measurement inaccuracies and model

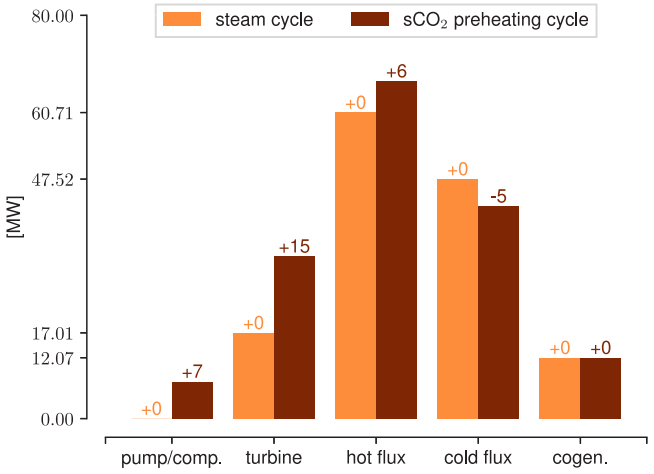

Fig. 8. The supercritical cycle recovers more heat in the exhaust gases and released less in the environment. The supercritical cycle presents more advantages towards waste heat recovery.

simplifications (e.g., exhaust gases cleaning unit, heat losses, additional pumps). Nonetheless, the comparison with sCO_2 remains relevant, providing a qualitative assessment of the differences between the two cycles across various processes (heating, cooling, etc.).

From a broader perspective, three main distinctions between the two cycles account for the lower performance of the steam cycle. Firstly, the exhaust gases released into the stack are cooler with the sCO_2 configuration (<80 °C) compared to the steam reference (approximately 150 °C), resulting in an exergy loss of 1 to 2 MW. Secondly, the regulation of cogenerated steam for the neighboring company involves mixing hot steam with colder water in the steam reference, leading to direct exergy destruction, albeit at a lower rate (less than 1 MW). The third and main reason behind the superior performance of the sCO_2 cycle lies in the sensible heat recovery of sCO_2 compared to the latent heat recovery of water at constant pressure. Specifically, sCO_2 achieves a higher temperature at the heater outlet (550 °C) compared to water in the steam configuration (420 °C), resulting in a recovered exergy up to 4–5 MW higher in the supercritical configuration.

While operating at higher temperatures enhances cycle efficiency, attention must be given to corrosion aspects, particularly cold and hot corrosion, in the heat exchangers. These aspects are duly considered and detailed in the off-design characterization.

The advantage of the sCO_2 configuration is evident, with a 7% higher cycle efficiency η achieved compared to the steam cycle. Excluding cogeneration, the supercritical cycle exhibits a mean efficiency of 36.2% (Fig. 9). Incorporating cogeneration elevates the efficiency to a mean value of 43.5%, with a maximum nearing 60% (Fig. 9).

3.2. Performances under off-design characteristics

The outcomes of the nominal simulation facilitate the identification (e.g., heat flux for exchangers) and description (e.g., exchanger area) of the specific characteristics that the various components must possess. To effectively model the exchangers, additional assumptions regarding thermal exchanges need to be established. Once the characteristics of the components and the control strategy are defined, the simulation results are subsequently presented.

While the off-design behavior of the components are considered in the simulation, it should be noted that the full transient effect are not taken into account. The simulation indeed focuses on an hourly evolution of the data and assumes that the components work at constant conditions during one hour. This limitation therefore implies that the instantaneous evolution of the components' characteristics are not investigated but averaged during one hour. Nevertheless this approximation allows to significantly reduce the computation time while still giving a pretty good estimation of the performances of the setup.

3.2.1. Off-design behavior of the components

Compressor. Based on the nominal simulation results, the compressor encounters a mass flow rate ranging from 155 kg/s to 318 kg/s. The compressor characteristics, depicted in Fig. 5, show its operation across a range of 0.45 to 1.7 times the nominal flow rate. Opting for a nominal flow rate of 220 kg/s appears to be the most appropriate choice, ensuring consistent margins relative to the minimum and maximum limits. The parameter Δh_{nom} is set at 26 kJ/kg, with Inlet Guide Vanes (IGV) controlled to maximize power output.

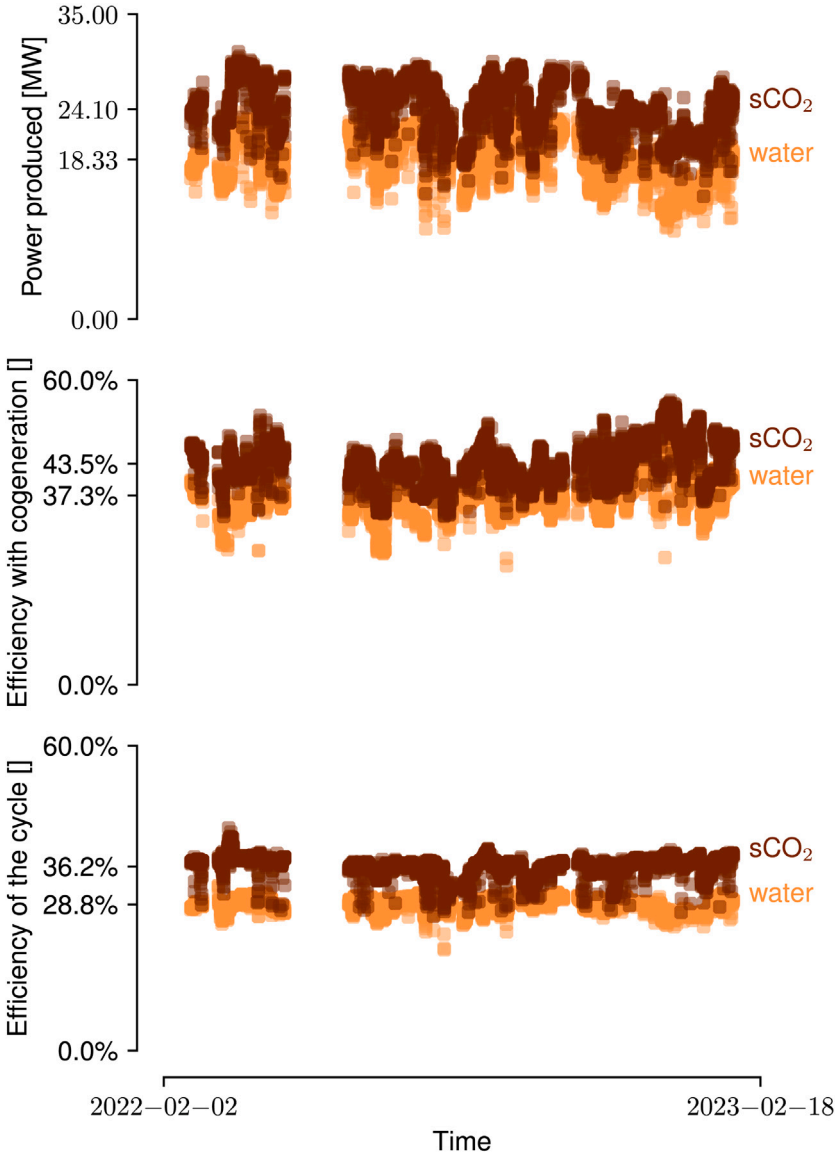

Fig. 9. On the one-year time frame, the preheating cycle has produced 5.8 MW_e more power and has been 7% more efficient than its steam counterpart when components are designed under their nominal performances. The preheating cycle has converted 44% of the heat recovered to power and cogenerated steam.

Turbine. For the turbine, it is assumed that the efficiency remains constant, given its negligible fluctuations as depicted in Fig. 6. The reference conditions are established for a nominal flow rate of 220 kg/s, a temperature of 600 °C, and a pressure of 280 bar. This results in a reduced mass flow rate of 11.6 kg $°K^{0.5}$ s^{-1} bar^{-1}. The normalized pressure ratio varies quadratically with the normalized reduced mass flow rate, following the expression presented in Eq. (14).

$$\frac{\Pi}{\Pi_{\text{ref}}} = 3.699\left(\frac{\dot{m}_{\text{red}}}{\dot{m}_{\text{red, ref}}}\right)^2 - 5.159\left(\frac{\dot{m}_{\text{red}}}{\dot{m}_{\text{red, ref}}}\right) + 2.458 \tag{14}$$

Heat exchangers. Within the heat exchangers, the overall thermal resistance (R) arises from the cumulative effect of resistances at both the cold (R_{cold}) and hot (R_{hot}) sides, under the assumption of ideal metal conductivity separating the two streams. Aspen Plus [27] offers the capability to incorporate power laws for modeling heat exchangers, with reference values outlined in Eq. (15). This enables the expression of the overall resistance using thermal transmittances (Eq. (16)), facilitating the integration of the Nusselt number into the equations.

$$\frac{U}{U_{\text{ref}}} = \left(\frac{\dot{m}_{\text{hot}}}{\dot{m}_{\text{hot, ref}}}\right)^a \left(\frac{\dot{m}_{\text{cold}}}{\dot{m}_{\text{cold, ref}}}\right)^b \tag{15}$$

Table 7
The off-design characteristics of the exchanger are used for the semi-transient simulation.

Exchanger	Recuperator	Preheater LT	Preheater HT	Heater	
Minimal cold flow	116	37	37	155	kg/s
Cold side Reynolds exponent	0.71	0.8	0.8	0.8	–
Minimal hot flow	155	31	59	59	kg/s
Hot side Reynolds exponent	0.77	0.8	0.8	0.8	–
Maximal heat flux	92.5	8.6	17.2	66.5	MW
Minimal LMTD	10	30	30	30	°C
UA	9250	285	573	2217	kW/°C

$$R = R_{\text{cold}} + R_{\text{hot}} \leftrightarrow \frac{1}{U} = \frac{1}{U_{\text{cold}}} + \frac{1}{U_{\text{hot}}} \leftrightarrow U = \frac{U_{\text{cold}} U_{\text{hot}}}{U_{\text{cold}} + U_{\text{hot}}} \tag{16}$$

The expression given in Eq. (15) can be reformulated as shown in Eq. (17).

$$\frac{U}{U_{\text{ref}}} = \frac{U_{\text{cold}} U_{\text{hot}}}{U_{\text{cold, ref}} U_{\text{hot, ref}}} \frac{U_{\text{cold, ref}} + U_{\text{hot, ref}}}{U_{\text{cold}} + U_{\text{hot}}} \simeq \left(\frac{U_{\text{cold}}}{U_{\text{cold, ref}}}\right)\left(\frac{U_{\text{hot}}}{U_{\text{hot, ref}}}\right) \tag{17}$$

The Nusselt number (Eq. (18)) is commonly expressed as the product of Reynolds number (Eq. (19)) and Prandtl number (Eq. (20)) raised to a specific exponent. These formulations illustrate the proportional relationship between the thermal transmittance (U) and flow velocity (v), and consequently with mass flow rate ($\dot{m}$), as depicted in Eq. (21).

$$Nu = \frac{UL}{\lambda} = aRe^x Pr^y \tag{18}$$

$$Re = \frac{\rho v L}{\mu} \tag{19}$$

$$Pr = \frac{\mu c_p}{\lambda} \tag{20}$$

$$\begin{aligned} \frac{UL}{\lambda} = a\left(\frac{\rho v L}{\mu}\right)^x \left(\frac{\mu c_p}{\lambda}\right)^y \leftrightarrow U &= \left[\frac{\lambda}{L} a \left(\frac{\rho L}{\mu}\right)^x \left(\frac{\mu c_p}{\lambda}\right)^y\right] v^x \\ \leftrightarrow U &= \left[\frac{\lambda}{L} a \left(\frac{\rho L}{\mu}\right)^x \left(\frac{\mu c_p}{\lambda}\right)^y \left(\frac{1}{\rho A}\right)^x\right] \dot{m}^x \end{aligned} \tag{21}$$

Assuming that the first term of the product remains constant from the reference case, Eq. (22) can be simplified to Eq. (23). This expression clearly demonstrates that the ratio of the thermal transmittances varies with the ratio of the mass flow rates at the cold and hot sides. The exponents a and b of the power law (Eq. (15)) correspond respectively to the exponent x of the Reynolds number in the expressions of the Nusselt number characterizing the heat transfer at the cold/hot side.

$$\frac{U}{U_{\text{ref}}} \simeq \left(\frac{\left[\frac{\lambda}{L} a \left(\frac{\rho L}{\mu}\right)^x \left(\frac{\mu c_p}{\lambda}\right)^y \left(\frac{1}{\rho A}\right)^x\right] \dot{m}^x}{\left[\frac{\lambda}{L} a \left(\frac{\rho L}{\mu}\right)^x \left(\frac{\mu c_p}{\lambda}\right)^y \left(\frac{1}{\rho A}\right)^x\right]_{\text{ref}} \dot{m}^x_{\text{ref}}} \right)_{\text{cold}} \left(\frac{\left[\frac{\lambda}{L} a \left(\frac{\rho L}{\mu}\right)^x \left(\frac{\mu c_p}{\lambda}\right)^y \left(\frac{1}{\rho A}\right)^x\right] \dot{m}^x}{\left[\frac{\lambda}{L} a \left(\frac{\rho L}{\mu}\right)^x \left(\frac{\mu c_p}{\lambda}\right)^y \left(\frac{1}{\rho A}\right)^x\right]_{\text{ref}} \dot{m}^x_{\text{ref}}} \right)_{\text{hot}} \tag{22}$$

$$\frac{U}{U_{\text{ref}}} \simeq \left(\frac{\dot{m}^x}{\dot{m}^x_{\text{ref}}}\right)_{\text{cold}} \left(\frac{\dot{m}^x}{\dot{m}^x_{\text{ref}}}\right)_{\text{hot}} \tag{23}$$

The design of the heat exchangers adopts the most conservative assumption, ensuring they can fulfill their objectives even under the most unfavorable operating conditions, i.e., facilitating the exchange of heat. Consequently, each exchanger is characterized by its maximum heat transfer capacity to maintain prescribed temperature levels. The reference UA value is derived by dividing the maximum heat flux by the minimum Logarithmic Mean Temperature Difference (LMTD). Additionally, the exchangers are characterized by the minimum hot and cold flows observed during the entire simulation, serving as reference flow rates in Eq. (23). Off-design data for the exchangers are provided in Table 7.

Regarding pressure losses, they are standardized to 5 bar when sCO_2 operates at high pressure (heater, preheater, and hot side of the recuperator) and 2 bar when at low pressure (cold side of the recuperator and cooler). The head losses in the exhaust gases remain consistent with the values provided by the sensors for the initial steam cycle, typically a few mbar. It is assumed that the outlet temperature of 33 °C is consistently maintained in the cooler.

Considering the presence of sulphites and chlorides in the flue gas, material selection must adhere to corrosion constraints. In the initial steam cycle, steel oxidation limits the working temperature range, particularly evident at low (in the first preheater) or high temperatures (in the heater). In contrast, in the context of sCO_2, exchangers are constructed from nickel-based superalloys, effectively mitigating these risks, even when the wall temperature reaches 550 °C [4,30].

Table 8
During the off-design simulation, the conditions in the components evolve in the following ranges according to the off-design characteristics.

Item	min	max	Unit
Split ratio	69	80	%
sCO_2 flow rate	174	223	kg/s
Recuperator heat flux	62	116	MW
Cooler heat flux	31	49	MW
Heater heat flux	28	41	MW
Preheater after cleaning heat flux	4	11	MW
Preheater before cleaning heat flux	3	27	MW
Low pressure	79	95	bar
High pressure	251	293	bar

Piping, mixer and split. In this simulation, pressure losses in the pipes, mixer, and split are disregarded relative to the heat exchangers. This is because the heat exchangers represent the primary locations where head losses manifest within the cycles. As for the split, flow distribution is tailored to optimize plant performance, with the mass ratio directed to the preheater typically maintained between 70% and 80%.

3.2.2. Optimization of the performances and control strategy

To enhance the net power output of the cycle, three parameters can be managed: the mass flow rate throughout the cycle, the IGV angle at the compressor inlet, and the split ratio between the preheaters and the recuperator. Leveraging the compressor and turbine maps, the mass flow rate and IGV angles are adjusted to establish equilibrium among the various pressure levels within the cycle, particularly at the turbine outlet and compressor inlet. Subsequently, the split ratio serves as an additional degree of freedom to maximize cycle power production. These parameters are varied within the bounds defined by the respective components, such as the minimal and maximal flow in the compressor. Incorporating turbine and compressor maps, along with the off-design behavior of heat exchangers, enables to address all nonlinearities in the optimization process, ensuring that components maintain operational conditions. Due to the off-design characteristics of the components, the pressure levels, flow rates and heat fluxes are changing in the ranges presented in Table 8. Those values are the result of the fluctuations encountered in the thermal sources combined with the optimization strategy.

3.2.3. Comparison of the off-design performances of sCO_2 and steam

In semi-transient operation, the net power output of the cycle (Fig. 10) is slightly lower than that achieved in the nominal design (Fig. 9). Nevertheless, the performance of the sCO_2 system remains superior to that of steam. Compared to the nominal simulation, the off-design sCO_2 cycle generates approximately 1.2 MW_e less power on average. This minor discrepancy can be attributed to two opposing factors. On one hand, the inclusion of pressure losses and the utilization of performance maps notably diminish the performance levels attained in the nominal simulation. However, on the other hand, the over-sizing of the heat exchangers, resulting from the conservative assumptions earlier, serves to enhance power production by increasing the amount of recovered heat. In terms of simulated efficiencies, all values remain within a similar range across various operating strategies (Fig. 10).

Given the specificity of the case in terms of the characteristics related to the waste heat source and the combined heat requirement, the model can neither be directly validated nor compared with an existing model also designed for a waste incinerator. However, the energy production and efficiency evolutions are in line with the steam configuration and evolve in the same way although at a higher value due to the higher efficiency of the sCO_2 cycle. Referring to the literature, it has already been presented by Liu [10] that sCO_2 cycles can be expected to achieve efficiencies close to 44% in combined heat and power applications. With these two elements in mind, the sCO_2 model can therefore be validated both in terms of the level of efficiency obtained and the evolution of production.

Relative to the initial steam cycle, the sCO_2 configuration enables the generation of an additional 4.57 MW_e. It is worth noting that the net production of the supercritical cycle is more tightly concentrated around its mean value compared to the steam cycle, as evidenced by their respective standard deviations of 1.54 MW_e and 2.70 MW_e. Considering cycle efficiency, the mean efficiency of the sCO_2 cycle surpasses its steam counterpart by 6.8%, as depicted in Fig. 10. When considering the cogeneration aspect, the sCO_2 cycle achieves an efficiency of approximately 43%, whereas the steam cycle fluctuates around 37.3%. Thus, the supercritical cycle exhibits greater efficiency compared to the conventional steam cycle. From an exergetic standpoint, the sCO_2 cycle converts 61.8% of the available exergy in the gases post-incineration (Eq. (13)). Consequently, the supercritical cycle is capable of generating more power while adhering to imposed constraints, namely cogeneration demands and temperature-based cleaning requirements.

3.3. Cost estimation

Due to the compact nature of supercritical cycles, certain configurations necessitate fewer components compared to their steam counterparts, thereby offering economic advantages. As elucidated by Weiland [31], the costs associated with these components can be correlated using a power law (Eq. (24)). Furthermore, Weiland has observed a temperature breakpoint around 550 °C. Beyond this threshold, nickel-based superalloys emerge as the most suitable materials, albeit at a higher cost compared to low-cost stainless

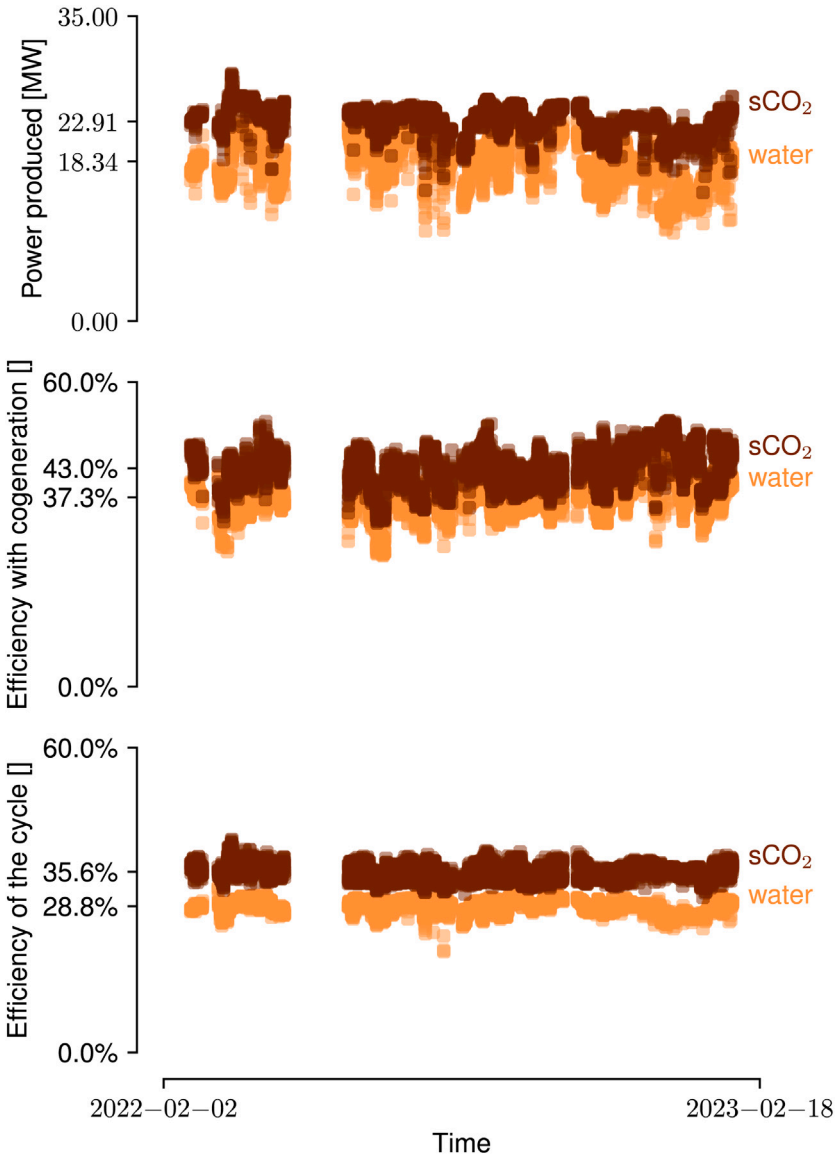

Fig. 10. 4.6 MW_e more power is produced and 6.8% of efficiency is gained by the sCO_2 cycle when the off-design behavior of the components is taken into account. The preheating cycle presents similar efficiency both under nominal and off-design characteristics.

steel alternatives, owing to their superior corrosion resistance. Consequently, when operating at temperatures exceeding 550 °C, a temperature correction factor f_T should be implemented, which increases quadratically with temperature.

$$C = a\, SP^b\, f_T \text{ [31]} \tag{24}$$

In the cost evaluation, the CEPCI has been adjusted from 2017 (567.5) to align with the 2022 value (813). As indicated in Table 9, the total capital expenditure for the plant, upon transitioning from a steam cycle to an sCO_2 cycle, escalates to 75.57 M$ with total uncertainties ranging from −30.0% to 37.2%. These uncertainties hinge on the availability of manufacturing technologies, spanning from mass production for common and affordable components to bespoke production for intricate and costly ones. Even if the uncertainties on the total costs are significant, the range calculated gives an idea of the investment required to develop these cycles, making it possible to compare them with other technologies (namely steam and organic cycles). Although the average value can be considered a fair estimate, the coming decades will allow us to refine the calculations and find out which of the upper or lower limits is more tangible. Despite the high uncertainty, it does not automatically mean that the results are not useful. In the opposite, it shows that there is a lot of potential but due to the lack of maturity, it is hard to say at this stage how much can be gained exactly.

Table 9
The work of Weiland [31] allows to assess boundaries for the cost of the different components.

Components	SP	Unit	a	b	Uncertainty		Cost M$		
					min	max	min	Mean	max
Recuperator	9.25×10^{6}	W/K	49.45	0.7544	−25%	28%	9.56	12.75	16.32
Preheater 1	8.60×10^{0}	MW	820 800	0.7327	−23%	26%	4.38	5.69	7.17
Preheater 2	1.72×10^{1}	MW	820 800	0.7237	−23%	26%	7.28	9.45	11.91
Heater	6.65×10^{1}	MW	820 800	0.7237	−23%	26%	19.61	25.46	32.09
Cooler	4.60×10^{6}	W/K	32.88	0.75	−25%	28%	3.51	4.68	5.99
Turbine	3.51×10^{1}	MW	182 600	0.5561	−25%	30%	1.42	1.89	2.46
Compressor	7.05×10^{0}	MW	1 230 000	0.3992	−40%	48%	2.31	3.84	5.69
Subtotal							48.07	63.77	81.62
Additional cost							10.0%	18.5%	27.0%
Total							52.87	75.57	103.66

Assuming all investments are executed at the plant's inception (with an 11% discount rate, a 15-year lifespan, and a 90% utilization ratio), the LCOE fluctuates between 8.51 $/MWh$_e$ and 16.69 $/MWh$_e$, contingent upon manufacturing costs, which stem from availability considerations. The average LCOE of 12.17 $/MWh$_e$ can be benchmarked against other energy production systems. However, it is crucial to acknowledge that this value is tied to a waste incinerator setting. Primarily, the plant's primary objective is the thermal destruction of municipal waste, rather than electricity production. Consequently, the bulk of maintenance expenses refers to the incinerator plant itself and is unrelated to electricity generation. Moreover, the energy source (i.e., municipal waste) is deemed cost-free, positively influencing the LCOE. Additionally, the financial significance of the cogenerated steam exported to the neighboring plant, alongside the costs associated with the steam generator responsible for its production, warrants consideration.

4. Future work

In the study presented in this paper, the behavior of an sCO$_2$ cycle was simulated in an innovative way, taking into account the off-design characteristics of the components, some work has been left for future improvements. In order to improve the accuracy of the model, all the auxiliary equipments can be added even if they will not significantly change the results of the simulation. Looking at the cooling unit, it has been indeed shown by Moisseytsev [24] that the consumption of the fans is expected to be lower than for a steam cycle. Taking into account their consumptions will thus also benefit to the supercritical setup. Regarding to the components for sCO$_2$ cycles, the off-design performances have been derived from dimensionless performance maps. While those curves already give a good idea of the evolution of the performances, it would have be ideal to take curves for components with a size that directly suits the considered application. Even though this kind of data is not massively present in literature, we can hope that the development of supercritical CO$_2$ cycles will bring in the coming years more information about the behavior of their components. Furthermore, the years ahead will also allow to refine the cost estimation of the supercritical components making then economic estimation more accurate.

5. Conclusions

In the context of the ongoing energy transition, waste heat recovery emerges as a promising way of valorizing the energy content of the exhaust gases with combined heat and power purposes. While steam cycles currently dominate that landscape, sCO$_2$ cycles position themselves as potential contenders to traditional setups due to their heightened heat recovery potential and the compactness facilitated by the supercritical state.

However, the literature lacks numerical examples substantiating the advantages of sCO$_2$ cycles and the assessment of the off-design performance of a waste incinerator based on a one-year data frame has never been investigated. Building on the CO$_2$OLHEAT consortium's efforts, a replication study involving a waste incinerator has been conducted to transition from an existing steam and power cogeneration setup to an sCO$_2$ cycle. Utilizing one year of hourly operational data, the replacement of the initial steam cycle with an sCO$_2$ configuration (with split flow and preheating) demonstrated a 4.6 MW$_e$ increase in power production compared to its steam-based predecessor. This translates to a global efficiency of 43%. In terms of economic viability, the selected sCO$_2$ cycle yields a LCOE ranging between 8.51 and 16.69 $/MWh$_e$.

The demonstrated benefits of supercritical power cycle technology for waste heat recovery underscore its potential for increased net power output, cost-effectiveness of installations, and the compact nature of turbomachinery. Moving ahead, it is imperative to refine existing heat exchanger models to better simulate heat transfer and head losses. Additionally, designing control algorithms and maintenance strategies should be focal points of future studies, alongside enhancing heat recovery methods, such as tapping into remaining heat potential in the cooler.

In a nutshell, the main findings of this study bring novelty to literature given that:

- an sCO$_2$ cycle has been designed and simulated over one year with the off-design characteristics of the components;
- the sCO$_2$ setup produces 4.6 MW$_e$ more power than the steam cycle, with a cogeneration requirement that is always met;
- the sCO$_2$ setup achieves a global efficiency of 43%;
- the average LCOE reaches 12.17 $/MWh$_e$.

CRediT authorship contribution statement

Vincent Thielens: Writing – original draft, Software, Methodology, Investigation, Formal analysis, Data curation, Conceptualization. **Frederiek Demeyer:** Writing – review & editing, Supervision, Project administration, Funding acquisition. **Ward De Paepe:** Writing – review & editing, Supervision, Project administration.

Declaration of competing interest

The authors declare that they have no known competing financial interests or personal relationships that could have appeared to influence the work reported in this paper.

Data availability

The data that has been used is confidential.

Declaration of Generative AI and AI-assisted technologies in the writing process

During the preparation of this work the author(s) used chatGPT 3.5 in order to improve readability and language of the text. After using this tool/service, the author(s) reviewed and edited the content as needed and take(s) full responsibility for the content of the publication.

Acknowledgments

This research is funded by the Belgian Fund for Scientific Research (F.R.S.-FNRS). Vincent Thielens is a Research Fellow of the Fonds de la Recherche Scientifique - FNRS.

References

[1] I. Johnson, W.T. Choate, A. Davidson, Waste heat recovery. Technology and opportunities in US industry, 2008.
[2] M.T. White, G. Bianchi, L. Chai, S.A. Tassou, A.I. Sayma, Review of supercritical CO2 technologies and systems for power generation, Appl. Therm. Eng. 185 (2021) 116447, http://dx.doi.org/10.1016/j.applthermaleng.2020.116447, URL https://www.sciencedirect.com/science/article/pii/S1359431120339235.
[3] S.A. Wright, C.S. Davidson, W.O. Scammell, Thermo-economic analysis of four sCO2 waste heat recovery power systems, in: Fifth International SCO2 Symposium, San Antonio, TX, Mar, 2016, pp. 28–31.
[4] K. Brun, P. Friedman, R. Dennis, Fundamentals and Applications of Supercritical Carbon Dioxide (sCO2) Based Power Cycles, Woodhead Publishing, 2017.
[5] D. Alfani, M. Binotti, E. Macchi, P. Silva, M. Astolfi, sCO2 power plants for waste heat recovery: design optimization and part-load operation strategies, Appl. Therm. Eng. 195 (2021-08) 117013, http://dx.doi.org/10.1016/j.applthermaleng.2021.117013, URL https://linkinghub.elsevier.com/retrieve/pii/S1359431121004592.
[6] S.A. Wright, C.S. Davidson, C. Husa, Off-design performance modeling results for a supercritical CO2 waste heat recovery power system, in: The 6th Supercritical CO2 Power Cycles Symposium, 2018.
[7] R. Sun, M. Liu, X. Chen, K. Yang, J. Yan, Thermodynamic optimization on supercritical carbon dioxide Brayton cycles to achieve combined heat and power generation, Energy Convers. Manage. 251 (2022) 114929.
[8] H. Chen, M. Zhang, Y. Wu, G. Xu, W. Liu, T. Liu, Design and performance evaluation of a new waste incineration power system integrated with a supercritical CO2 power cycle and a coal-fired power plant, Energy Convers. Manag. 210 (2020) 112715.
[9] M. Baggiani, P. Bruttini, A. Cagnac, Y. De Vos, S. Glos, G. Persico, J. Spolcova, R. Le Pierres, G. Messina, S. Tassou, Supporting document for the CO2OLHEAT technical poster presented during the supercritical CO2 power cycles symposium (21 feb – 24 feb 2022, San Antonio, Texas, USA), 2022-02-21, p. 12.
[10] M. Liu, X. Zhang, Y. Ma, J. Yan, Thermo-economic analyses on a new conceptual system of waste heat recovery integrated with an S-CO2 cycle for coal-fired power plants, Energy Convers Manag 161 (2018) 243–253.
[11] F. Crespi, G. Gavagnin, D. Sánchez, G.S. Martínez, Supercritical carbon dioxide cycles for power generation: A review, Appl. Energy 195 (2017-06) 152–183, http://dx.doi.org/10.1016/j.apenergy.2017.02.048, URL https://linkinghub.elsevier.com/retrieve/pii/S0306261917301915.
[12] D. Alfani, M. Astolfi, P. Silva, G. Persico, Technical report: Off design performance of the sCO2 power unit connected to the cement plant heat recovery, 2022-06-23, p. 24.
[13] Y. Ahn, S.J. Bae, M. Kim, S.K. Cho, S. Baik, J.I. Lee, J.E. Cha, Review of supercritical CO2 power cycle technology and current status of research and development, Nucl. Eng. Technol. 47 (6) (2015) 647–661, Publisher: Elsevier.
[14] M. Penkuhn, G. Tsatsaronis, A decomposition method for the evaluation of component interactions in energy conversion systems for application to advanced exergy-based analyses, Energy 133 (2017) 388–403, Publisher: Elsevier.
[15] E. Krasnoshchekov, Experimental study of heat exchagne in carbon dioxide in the supercritical range at high temperature drops, High Temp. 4 (1966) 375–382.
[16] J. Jackson, Fluid flow and convective heat transfer to fluids at supercritical pressure, Nucl. Eng. Des. 264 (2013) 24–40, Publisher: Elsevier.
[17] W. Kast, (Revised by Hermann Nirschl), E.S. Gaddis, K.-E. Wirth, J. Stichlmair, L1 pressure drop in single phase flow, in: VDI Heat Atlas, Springer Berlin Heidelberg, 2010, pp. 1053–1116, http://dx.doi.org/10.1007/978-3-540-77877-6_70.
[18] J.S. Kwon, S. Son, J.Y. Heo, J.I. Lee, Compact heat exchangers for supercritical CO2 power cycle application, Energy Convers. Manage. 209 (2020) 112666, Publisher: Elsevier.
[19] V. Gnielinski, G6 heat transfer in cross-flow around single tubes, wires, and profiled cylinders, in: VDI Heat Atlas, in: VDI-Buch, Springer, 2010, pp. 723–724, http://dx.doi.org/10.1007/978-3-540-77877-6_39.
[20] D.E. Kim, M.H. Kim, J.E. Cha, S.O. Kim, Numerical investigation on thermal–hydraulic performance of new printed circuit heat exchanger model, Nucl. Eng. Des. 238 (12) (2008) 3269–3276, Publisher: Elsevier.
[21] N. Tsuzuki, Y. Kato, K. Nikitin, T. Ishizuka, Advanced microchannel heat exchanger with S-shaped fins, J. Nucl. Sci. Technol. 46 (5) (2009) 403–412, Publisher: Taylor & Francis.

[22] A. Meshram, A.K. Jaiswal, S.D. Khivsara, J.D. Ortega, C. Ho, R. Bapat, P. Dutta, Modeling and analysis of a printed circuit heat exchanger for supercritical CO2 power cycle applications, Appl. Therm. Eng. 109 (2016) 861–870, Publisher: Elsevier.
[23] P. Fourspring, J. Nehrbauer, S. Sullivan, J. Nash, Testing of compact recuperators for a supercritical CO2 Brayton power cycle, in: Proceedings of the 4th International Symposium on Supercritical CO2 Power Cycles, 2014.
[24] A. Moisseytsev, Q. Lv, J.J. Sienicki, Heat exchanger options for dry air cooling for the sco2 Brayton cycle, in: Turbo Expo: Power for Land, Sea, and Air, vol. 50961, American Society of Mechanical Engineers, 2017, V009T38A006.
[25] R. Span, W. Wagner, A new equation of state for carbon dioxide covering the fluid region from the triple-point temperature to 1100 K at pressures up to 800 MPa, J. Phys. Chem. Ref. Data 25 (6) (1996-11) 1509–1596, http://dx.doi.org/10.1063/1.555991, URL http://aip.scitation.org/doi/10.1063/1.555991.
[26] C.W. White, N.T. Weiland, Evaluation of property methods for modeling direct-supercritical CO2 power cycles, J. Eng. Gas Turb. Power 140 (1) (2018-01-01) 011701, http://dx.doi.org/10.1115/1.4037665, URL https://asmedigitalcollection.asme.org/gasturbinespower/article/doi/10.1115/1.4037665/374499/Evaluation-of-Property-Methods-for-Modeling.
[27] AspenTech, Asset performance management solution. URL https://www.aspentech.com/en/solutions/asset-performance-management.
[28] I. Dincer, M.A. Rosen, Chapter 1 - thermodynamic fundamentals, in: I. Dincer, M.A. Rosen (Eds.), Exergy (Second Edition), second ed., Elsevier, 2013, pp. 1–20, http://dx.doi.org/10.1016/B978-0-08-097089-9.00001-2, URL https://www.sciencedirect.com/science/article/pii/B9780080970899000012.
[29] I. Dincer, M.A. Rosen, Chapter 2 - exergy and energy analyses, in: I. Dincer, M.A. Rosen (Eds.), Exergy (Second Edition), second ed., Elsevier, 2013, pp. 21–30, http://dx.doi.org/10.1016/B978-0-08-097089-9.00002-4, URL https://www.sciencedirect.com/science/article/pii/B9780080970899000024.
[30] S.-H. Lee, N.J. Themelis, M.J. Castaldi, High-temperature corrosion in waste-to-energy boilers, J. Therm. Spray Technol. 16 (2007) 104–110.
[31] N.T. Weiland, B.W. Lance, S.R. Pidaparti, SCO2 power cycle component cost correlations from DOE data spanning multiple scales and applications, in: Turbo Expo: Power for Land, Sea, and Air, Vol. 58721, American Society of Mechanical Engineers, 2019, V009T38A008.